Parametric study of multi-armed jets

Artur Tyliszczak

Department of Mechanical Engineering and Computer Science.
Czestochowa University of Technology
Al. Armii Krajowej 21, 42-201 Czestochowa, Poland
email: atyl@imc.pcz.pl

ABSTRACT

The paper presents the results of numerical simulations of excited jets in which the excitation is obtained through the addition of an axial and helical forcing to an inlet velocity. The research is performed using direct numerical simulations (DNS) and high-order numerical code. It is shown that by a proper choice of the ratio of axial and helical frequencies different type of multi-armed jets can be created, eg. with 5th, 7th, 8th, 12th, 13th branches. It is observed that the angle at which the branches disjoin from the main jet and the axial location where this phenomenon starts are related to the axial forcing frequency.

INTRODUCTION

Interest in flow control techniques is driven by a possible improvement of performance, safety and efficiency of various technical devices. Existing strategies of steering and controlling fluid flows can be divided into two approaches: passive and active. The former are based on shaping of flow domain and usually are optimized for specific flow conditions. The latter require external energy input which can be varying in response to the instantaneous flow behaviour. The active methods are thus more costly but also much more flexible. Under a variety of different flow regimes they result in a better overall response than the passive methods. In this work we concentrate on active control of a jet flow and focus on fundamental aspects of its dynamics. However, the performed research is valuable also for engineers as the analyzed configuration has many practical applications (burners, rocket nozzle, injectors etc.). The research devoted to active jet control was initiated in the 70s by a study of Crow and Champagne (1971). It was shown that, with a properly chosen forcing (excitation), a jet changes its qualitative behaviour compared to the natural unexcited jet. It was observed that turbulence intensity and mixing was significantly increased. Spectacular examples of excited jets occurring for a particular forcing method were discovered in early 80s and were called bifurcating and blooming jets. The former are characterized by occurrence of two well defined separate branches with vortex rings traveling along the branches, and the latter by a chaotic motion of the vortices (Parekh et al. 1988; Reynolds et al. 2003).

A recent work by Tyliszczak (2015a) showed that, apart from the above mentioned jets, different types of multi-armed jets are likely to occur. They reveal as the jets with distinct branches (e.g. 5 or 12) disjoining from the main jet stream a few diameters downstream a nozzle exit. Similarly as blooming jets the multi-armed ones are obtained through axial and helical excitations superimposed on an inlet velocity profile, but with specific settings of axial (f_a) to helical (f_h) forcing frequency ratios. In this paper DNS studies concerning an influence of f_a/f_h and f_a on a characteristics of the multi-armed jets are performed. It is found that with a particular setting of f_a/f_h the multi-armed jets with 5th, 7th, 8th, 12th, 13th branches can be created and that changing f_a alters a strength of the splitting phenomenon, its spatial location and angle at which the branches disjoin from the main jet.

MODELLING

We consider an incompressible flow with a constant density and constant temperature. The applied DNS solver is an in-house high-order code called SAILOR. The solution algorithm used in the SAILOR code is based on the projection method for pressure-velocity coupling. The time integration is performed using the Adams-Bashforth / Adams-Multon predictor-corrector method and the spatial discretization is performed using the 6th order compact difference method for half-staggered meshes (Tyliszczak, 2014; Tyliszczak, 2016). The velocity nodes are common for all three velocity components whereas the pressure nodes are moved half a grid size from the velocity nodes. This greatly facilitates implementation of the code and is computationally efficient as there is only a small amount of interpolation between the nodes. The staggering of the pressure nodes is sufficient to ensure a strong velocity-pressure coupling which eliminates the well known pressure oscillations occurring on collocated meshes.

The SAILOR code has been verified and validated both in problems with wall bounded flow domains and in free flows, including classical and excited jets and flames (Tyliszczak and Geurts, 2014; Tyliszczak and Geurts, 2015, Tyliszczak, 2015a; Tyliszczak, 2015b). In all these cases, the SAILOR code turned out to be computationally very efficient and accurate. This is expected to carry over to the simulations performed in this paper as a complexity of the cases analyzed here is similar to the complexity of problems studied previously.

CASE CONFIGURATION

We consider circular jets at Reynolds numbers Re = 1000 and Re = 3000, with Re = $U_j D/\nu$ where U_j is the inlet centerline velocity, D - diameter of the jet nozzle, ν - kinematic viscosity. The flow set-up showing the jet nozzle together with a sketched excitation is presented in Fig. 1. In the present work the inner geometry of the nozzle and forcing generators are not considered. The analyzed domain is a simple rectangular box which starts in the plane of the nozzle exit and covers the region $12D \times 16D \times 12D$. This size is found large enough to capture the main flow features with only small influence of the side boundaries. The presence of forcing is mimicked by the inlet velocity profile $U(\mathbf{x},t)$ specified in terms of the mean velocity profile $U_0(\mathbf{x})$ to which forcing component is superimposed as:

$$\frac{U(\mathbf{x},t)}{U_0(\mathbf{x})} = 1 + A \left(\underbrace{\sin\left(2\pi f_a t\right)}_{\text{axial forcing}} + \underbrace{\sin\left(2\pi f_h t + \theta(\mathbf{x})\right)\sin\left(\pi r/D\right)}_{\text{helical forcing}} \right) \tag{1}$$

where A is the forcing amplitude. A spatial extent of the forcing is limited to the jet region only, i.e. $r \leq D/2$, where r measures the radial distance from the centerline. The mean streamwise velocity
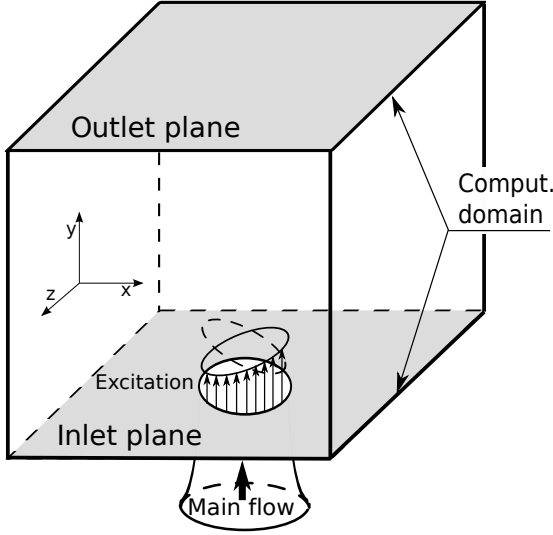
Figure 1. Schematic view of the computational domain.

is taken as the hyperbolic-tangent profile:

$$U_0(\mathbf{x}) = \frac{U_j + U_c}{2} - \frac{U_j - U_c}{2}\tanh\left(\frac{1}{4}\frac{R}{\delta_\theta}\left(\frac{r}{R} - \frac{R}{r}\right)\right) \quad (2)$$

The symbol U_c denotes a co-flow velocity added to mimic the natural suction and entrainment from surroundings, it is taken equal to $0.03U_j$. The symbol R is the nozzle radius and δ_θ is the momentum thickness of the initial shear layer. In all the cases presented in this paper the momentum thickness is $\delta_\theta = 0.05R$ which is the same as used by da Silva and Metais (2002), Tyliszczak and Geurts (2014), Tyliszczak (2015a). At the side boundaries the streamwise velocity is taken equal to the co-flow velocity U_c while the velocity components normal to the boundary of the domain are set equal to zero. The pressure at the inlet and side boundaries is computed using the Neumann condition $\partial p/\partial n = 0$. At the outlet plane the pressure is assumed constant and set equal to 0. All velocity components are computed from the convective boundary condition $\partial u_i/\partial t + C\partial u_i/\partial y = 0$ with C being the convection velocity which is computed as the (x,z) averaged mean velocity in the outlet plane, at every time step. This boundary condition is found to be stable and allows the flow structures to leave the domain with only small distortion.

The simulations have been performed on two computational meshes, the basic one consisted of $192 \times 264 \times 192$ nodes compacted in the radial direction using a tangent hyperbolic function and also axially towards the boundary side by an exponential function. The inlet region of the jet, i.e., $1D \times 1D$, was covered by 48×48 almost uniformly distributed nodes with $\Delta x = \Delta z \approx 0.02D$. In the axial direction the smallest was the first cell size, it had the length $\Delta y_{min} = 0.04D$. The second mesh was denser and was used to verify dependence of the results on the number of the computational nodes. These tests were performed only for some selected cases and the dense mesh consisted of $320 \times 384 \times 320$, the cell sizes were equal to $\Delta x = \Delta z \approx 0.013D$, $\Delta y_{min} = 0.028D$.

Excitation parameters

The excitation defined in Eq. (1) includes three control parameters which determine its strength and temporal frequency. As shown in Tyliszczak and Geurts (2014) the effect of the excitation is the most pronounced when the Strouhal number corresponding
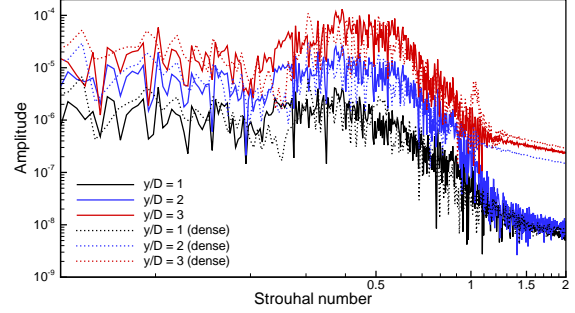

Figure 2. Axial velocity spectrum for unexcited jet for Re $= 3000$ at three distances from the inlet ($y/D = 1,2,3$). The results obtained on the coarse and dense meshes.

to the axial excitation frequency $St_a = f_a D/U_j$ is close to the preferred mode frequency and the amplitude of excitation is significantly larger than the level of natural turbulence intensity. In the present work we are interested mainly in large scale effects of the excitation and hence we assume that the turbulence intensity at the inlet is equal to zero and we take a relatively large amplitude of the excitation equal to $A = 0.15U_j$. Figure 2 shows amplitude spectra of the axial velocity component for unexcited jet for Re $= 3000$ at three distances from the inlet ($y/D = 1,2,3$). These results were obtained on the coarse and dense meshes and it can be seen that qualitatively they do not differ. Definitely there is no distinct peak that could be univocally related to a preferred mode frequency, however, a broadband region of increased fluctuations between $St = 0.3 - 0.6$ is well visible. This suggested to perform the computations with the axial forcing frequency corresponding to the whole this range. Hence, for Re $= 3000$ the computations have been carried out for $St_a = 0.30, 0.35, 0.40, 0.45, 0.50, 0.55$, whereas for Re $= 1000$ the simulations were limited only to the cases with $St_a = 0.45$. Assuming that the axial frequency has been selected the helical one is computed as $f_h = f_a/\alpha$ and we analyse the range of $1.5 \leq \alpha \leq 4.0$. As shown in Tyliszczak (2015a) the maxima of the excitations occur in the same azimuthal location $\theta = \pi/2(4n+1)(1-1/\alpha)$ for the time moments equal to $t_n = (4n+1)/(4f_a)$ for $n = 0,1,2,.....$ For instance, for $\alpha = 2$ in every single helical cycle the joint maxima occur at $\theta = \pi/4, 5\pi/4, \pi/4, \ldots$, and for $\alpha = 3$ at $\theta = \pi/3, 5\pi/3, \pi, \pi/3, \ldots$. An angular distance between two successive maxima is $\Delta\theta = 2\pi - (\theta_{n+1} - \theta_n) = 2\pi/\alpha$.

Let m denotes the number of helical cycles over which the joint maximum returns to its initial location at $\theta_{ini} = \pi/2(1 - 1/\alpha)$. The time when this happens is equal to $\Delta t_{\theta_{ini}} = N_\theta/f_a$. The symbol N_θ denotes the number of the azimuthal locations where the joint maxima occur, it is related to the excitation frequencies as $\alpha = N_\theta/m$. For instance for $m = 1$ one could expect that the combinations as $\alpha = 2/1$, $\alpha = 3/1$, $\alpha = 4/1$ will result in 2, 3 and 4 branches. Then, excluding repeating values of α (eg. $\alpha = 2/1 = 4/2 = 6/3$, etc.) for $m = 2$ with $\alpha = 3/2$, $\alpha = 5/2$, $\alpha = 7/2$ we should have 3, 5 and 7 branches, for $m = 4$ with $\alpha = 9/4$, $\alpha = 11/4$, $\alpha = 13/4$ it should be 9, 11, 13 branches, and for $m = 5$ with $\alpha = 11/5$, $\alpha = 12/5$, $\alpha = 13/5$ one could expect 11, 12 and 13 branches, respectively. Possibly, for $m > 5$ there are another combinations but they are not considered in the present studies. The performed parametric studies included all above mentioned combinations with additional values of α in the range $1.5 \leq \alpha \leq 4.0$ with $\Delta\alpha = 0.1$.

RESULTS

In all performed simulations the solution procedure was the same. Starting from quiescent initial conditions the jet with assumed excitation was injected into the computational domain and

developed freely. When the flow was found to be fully developed, approximately after a time $100D/U_j$, the time-averaging procedure started for the next $1000D/U_j$. This was certainly sufficient to show qualitative jet behaviors, but in some cases insufficient to say that the statistics were fully converged. Figure 3 shows axial velocity spectra obtained from the computations for excited jets for $Re = 3000$ with $St_a = 0.45$ and various α at three distances from the inlet $y/D = 0, 5, 7$ in the axis of the jets. It is seen that at the inlet only one distinct peak corresponding to the axial forcing is present. Note that in the axial locations the effect of the helical forcing is not present because it equals to zero at $r = 0$. Further downstream the jet becomes unstable, the natural Kelvin-Helmholtz instability mechanism interacts with the forcing and the flow become turbulent. This manifests by the presence of both larger and smaller frequencies in the spectra and also by a characteristic subharmonic peaks at $St = 0.45, 1.35, ...$ related to the paring process of the excited vortices. Note that differences resulting from various α values are small and only quantitative, i.e. there are no signs that a particular jet have been excited with $\alpha = 7/3$ while other with $\alpha = 9/4$. In all the cases the dominant subharmonic peaks overlap and differences can be found only at smaller amplitude levels.

These seemingly small differences in the spectra lead to very large differences in the flow behaviour. The jets for various α are visualized by an isosurface of the Q-parameter, $(Q = 0.5(U_j/D)^2)$ in Fig. 4. The Q-parameter is defined as $Q = \frac{1}{2}(S_{ij}S_{ij} - \Omega_{ij}\Omega_{ij})$ where S_{ij} and Ω_{ij} are symmetrical and antisymmetrical parts of the velocity gradient tensor. It is regarded as a very good indicator of organized vortical motion and here it clearly exhibits the toroidal vortices (rings) resulting from the excitation. Looking at their instantaneous positions, either from the side view or from the top view, it is difficult to recognize which forcing parameters were applied and whether there are any distinct branches, particularly for $\alpha \neq 2$. It is much easier to analyze the time-averaged results, hence, the presented figures show also the isosurface of the mean axial velocity. For the case with $\alpha = 2.0$ the scenario is as follows. The maxima of excitation occur alternately on opposite sides of the jet such that newly generated vortex amplifies the inclination of the preceding one. The vortices move downstream, roll-up and at $y/D \approx 4$ begin to flow along two distinct streams. Next the vortices which follow the same path start to behave as a shrinking spring and eventually break down. For $\alpha \neq 2.0$ the interactions between the vortices are more complex. In these cases, the successive rings are rotated by $\Delta\theta_\alpha \neq 180°$, and depending on α they mutually interact amplifying or destroying each other. Figure 4 shows sample case for which the separate branches are readily apparent and in which well defined vortex rings are visible even very far from the jet axis. Mechanism of their generation is the same for all α, for instances for $\alpha = 5/2$ during every $m = 2$ helical cycles there are $N_\theta = 5$ vortices that leave the jet nozzle, which move downstream into five distinct directions and form separate branches. The vortices in the branches survive as whole rings and break down only hitting the domain boundaries. The presented results show the jets with 3, 2, 5, 3, 7, 8, 11, 12 and 13 branches. Selected cross-section in $z − x$ planes at the location before the jet splitting at $y/D = 3$ and also further downstream at $y/D = 7$, where the separate branches have been formed, are shown in Fig. 5 presenting the contours of the axial velocity in the simulations for $St_a = 0.35$, $St_a = 0.45$ and $St_a = 0.55$. For the cases with $St_a = 0.45$ it can be seen that except for the case with $\alpha = 4/2$ the formed jets have regular elliptical shape with the longer axes oriented radially towards the jet axis. For the cases with $\alpha = 12/5$ and $\alpha = 13/5$ the jet borders at $y/D = 7$ are still connected, they separate completely only at the further distances. Interesting is that particular branches have more or less the same size, regardless of their number. In effect the maximum velocity
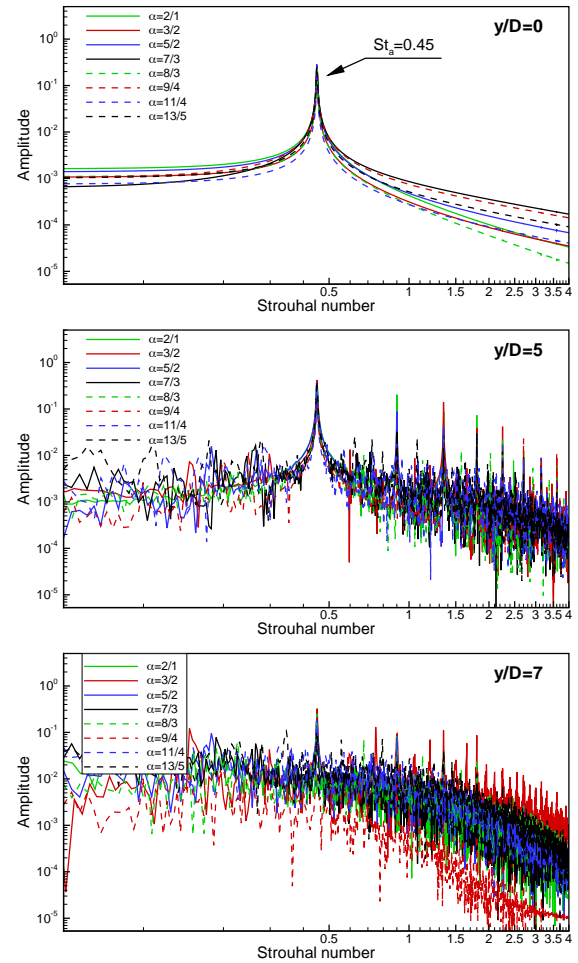

Figure 3. Axial velocity spectrum at $y/D = 0, 5, 7$ in the axis for excited jets for $Re = 3000$ with $St_a = 0.45$ and various α.

inside them changes substantially, and by the mass conservation, it becomes smaller when more streams are formed. Compared to the simulations for $St_a = 0.45$ the solutions obtained for $St_a = 0.35$ and $St_a = 0.55$ look significantly different. In the former case the jets do not divide, whereas for $St_a = 0.55$ the separate branches occur only for $\alpha = 4/2$ and $\alpha = 5/2$. However, unlike in the case with $St_a = 0.45$ the five branches obtained for $\alpha = 5/2$ are connected to the main jet stream. Moreover, their shape is not elliptical anymore, but it rather reminds a propeller.

Different splittings of the jets obviously lead to different flow behaviour in the jet axis. Figure 6 shows profiles of the time-averaged axial velocity along the axis for the results shown in Fig. 5. The region of the potential core, where the unexcited jets preserve their initial velocity at $y/D \leq 5$, is not present here. At the distance $y/D \leq 3$ velocity decreases smoothly, the solutions are very similarly and seem only weakly dependent on the forcing frequencies. Downstream, in the cases in which the strong splitting occurs the velocity in the center of the domain drops very quickly and even below zero. This happens for the cases with $St_a = 0.45$ and $\alpha = 5/2, 8/3, 13/5$. Worth noting is that for $St_a = 0.55$ with $\alpha = 8/3, 13/5$ the opposite effect is observed. After the initial velocity decrease in the region $y/D \leq 3$ it increases substantially around $y/D = 6$.

Finally, Fig. 7 presents the results for $St_a = 0.35$ and $St_a = 0.55$ for which the jet splitting was observed. It can be seen that the forcing frequency significantly affects an angle between the jet axis

(a) $\alpha = 3/2$ (b) $\alpha = 4/2$ (c) $\alpha = 5/2$

(d) $\alpha = 6/2$ (e) $\alpha = 7/3$ (f) $\alpha = 8/3$

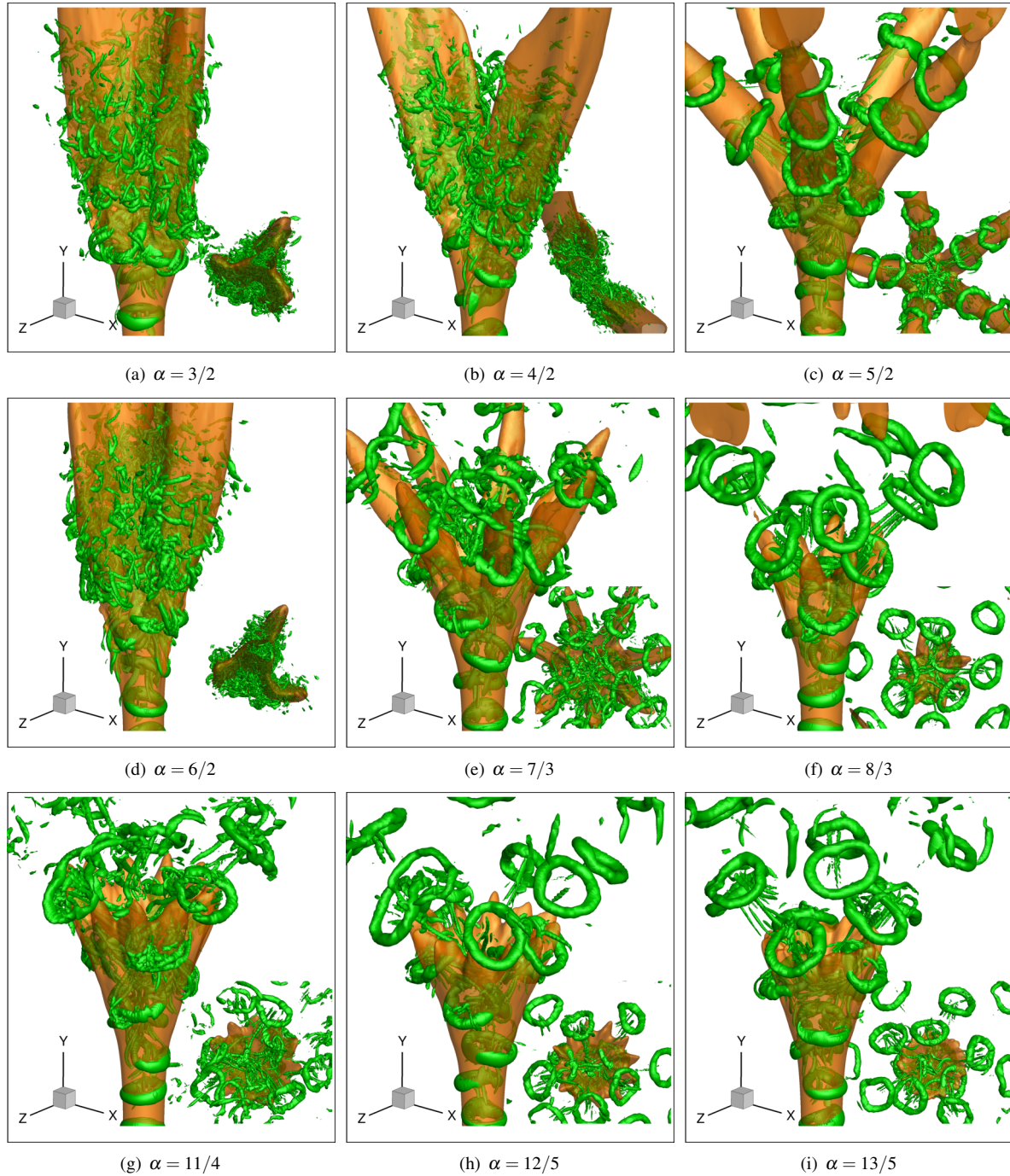(g) $\alpha = 11/4$ (h) $\alpha = 12/5$ (i) $\alpha = 13/5$

Figure 4. Isosurfaces of the time-averaged axial velocity ($\langle U \rangle = 0.2U_j$, orange) and instantaneous Q-parameter ($Q = 0.5(U_j/D)^2$, green). The results obtained for Re $= 3000$ with the excitation at St$_a = 0.45$ and various α.

and the branches. For instance, comparing the presented results with the solutions shown in Fig. 4 one may observe that for $\alpha = 4/2, 5/2$ this angle is the largest for St$_a = 0.45$. On the other hand, for $\alpha = 3/2$ the jet clearly splits only for St$_a = 0.35$, while for $\alpha = 4$ with St$_a = 0.55$ the jet exhibits a cross-like shape.

CONCLUSIONS

The paper presented numerical simulations of multi-armed jets obtained through the axial and helical excitations superimposed on the inlet velocity profile. The research was performed using a high-order compact method applying DNS approach for Re $= 1000$ and Re $= 3000$. In the present paper only the results for the latter were presented. It was observed that the solutions for Re $= 1000$ show

similar trends but differ quantitatively. It was demonstrated that by a proper choice of the ratio of axial and helical frequencies different type of multi-armed jets can be created with 5th, 7th, 8th, 12th, 13th branches. The angle at which the branches disjoin from the main jet and the axial location where this phenomenon starts are related directly to the axial forcing frequency.
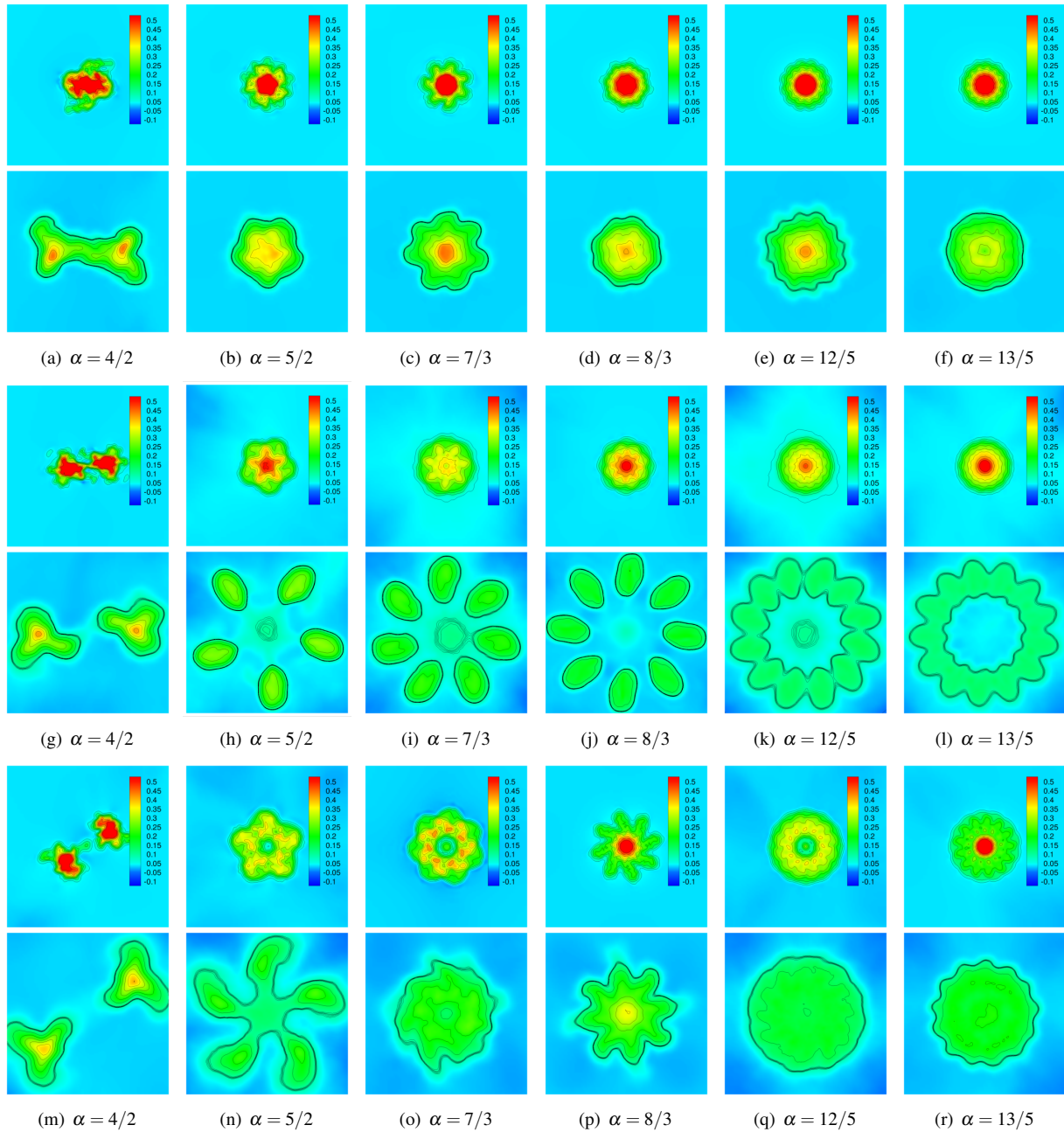
Acknowledgments

Figure 5. Contours of the time-averaged axial velocity for Re = 3000 in the cross-sections at $y/D = 3$ and $y/D = 7$. The excitation with various α for $\mathrm{St}_a = 0.35$ (upper row), $\mathrm{St}_a = 0.45$ (central row) and $\mathrm{St}_a = 0.55$ (bottom row).

REFERENCES

Crow, S.C., Champagne, F.H., 1971, "Orderly structure in jet turbulence", Journal of Fluid Mechanics, Vol. 48, pp. 547-691.

Reynolds, W.C., Parekh, D.E., Juvet, P.J.D., Lee, M.J.D., 2003, "Bifurcating and blooming jets", Annual Review of Fluid Mechanics, Vol. 35, pp. 295-315.

Parekh, D., Leonard, A., Reynolds W.C., 1988, "Bifurcating jets at high Reynolds number", Technical Report TF-35, Stanford University.

Tyliszczak, A., 2015a, "Multi-armed jets: A subset of the blooming jets", Physics of Fluids, Vol. 27 (041703), pp. 1-7.

Tyliszczak, A., 2014, "A high-order compact difference algorithm for half-staggered grids for laminar and turbulent incompressible flows", Journal of Computational Physics, Vol. 276, pp. 438-467.

Tyliszczak, A., 2016, "High-order compact difference algorithm on half-staggered meshes for low Mach number flows", Computers and Fluids, Vol. 127, pp. 131-145.

Tyliszczak, A., Geurts, B.J., 2014, "Parametric analysis of excited round jets - numerical study", Flow, Turbulence and Combustion, Vol. 93, pp. 221-247.

Tyliszczak, A., Geurts, B.J., 2015, "Controlled mixing enhancement in turbulent rectangular jets responding to periodically forced inflow conditions", Journal of Turbulence, Vol. 16, pp. 742-771.

Tyliszczak, A., 2015b, "LES-CMC of excited hydrogen jet", Combustion and Flame, Vol. 162, pp. 3864-3883.

da Silva, C.B., Métais, O., 2002, "Vortex control of bifurcating jets: A numerical ", Physics of Fluids, Vol. 14, pp. 3798-3819.
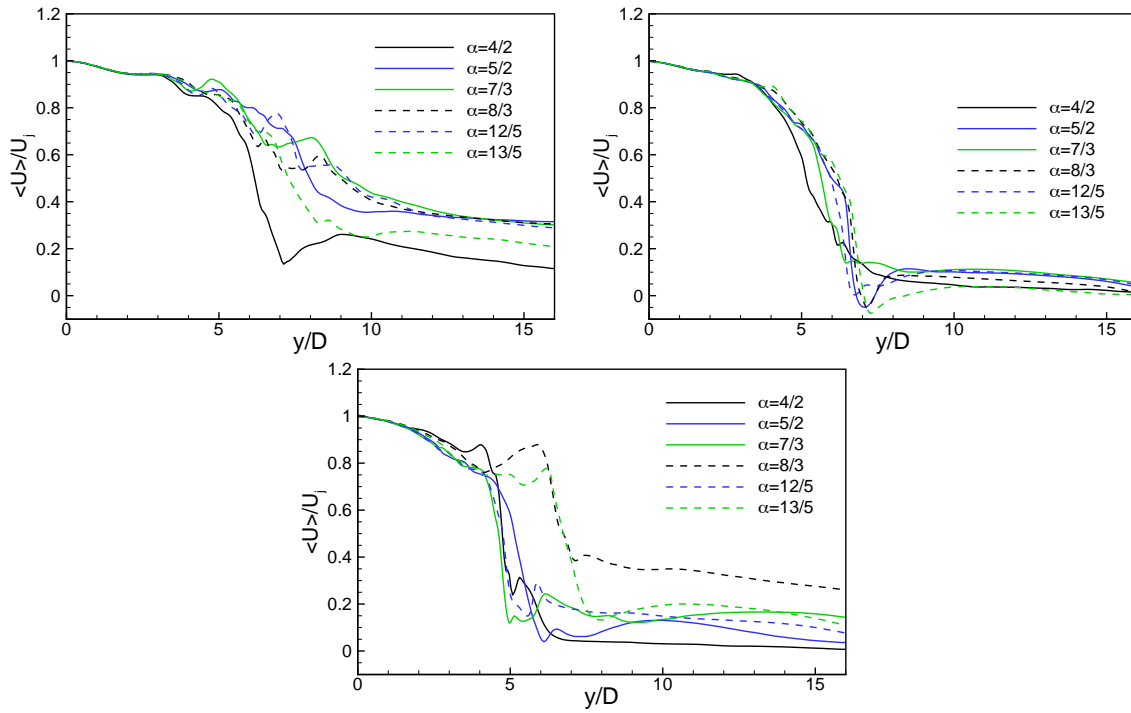
Figure 6. Axial velocity profiles along the jet axis for excited jets for $Re = 3000$ with $St_a = 0.35, 0.45$ and 0.55 for various α.

(a) $\alpha = 3/2$, $St_a = 0.35$

(b) $\alpha = 4/2$, $St_a = 0.35$

(c) $\alpha = 8/5$, $St_a = 0.35$

(d) $\alpha = 4/2$, $St_a = 0.55$

(e) $\alpha = 5/2$, $St_a = 0.55$
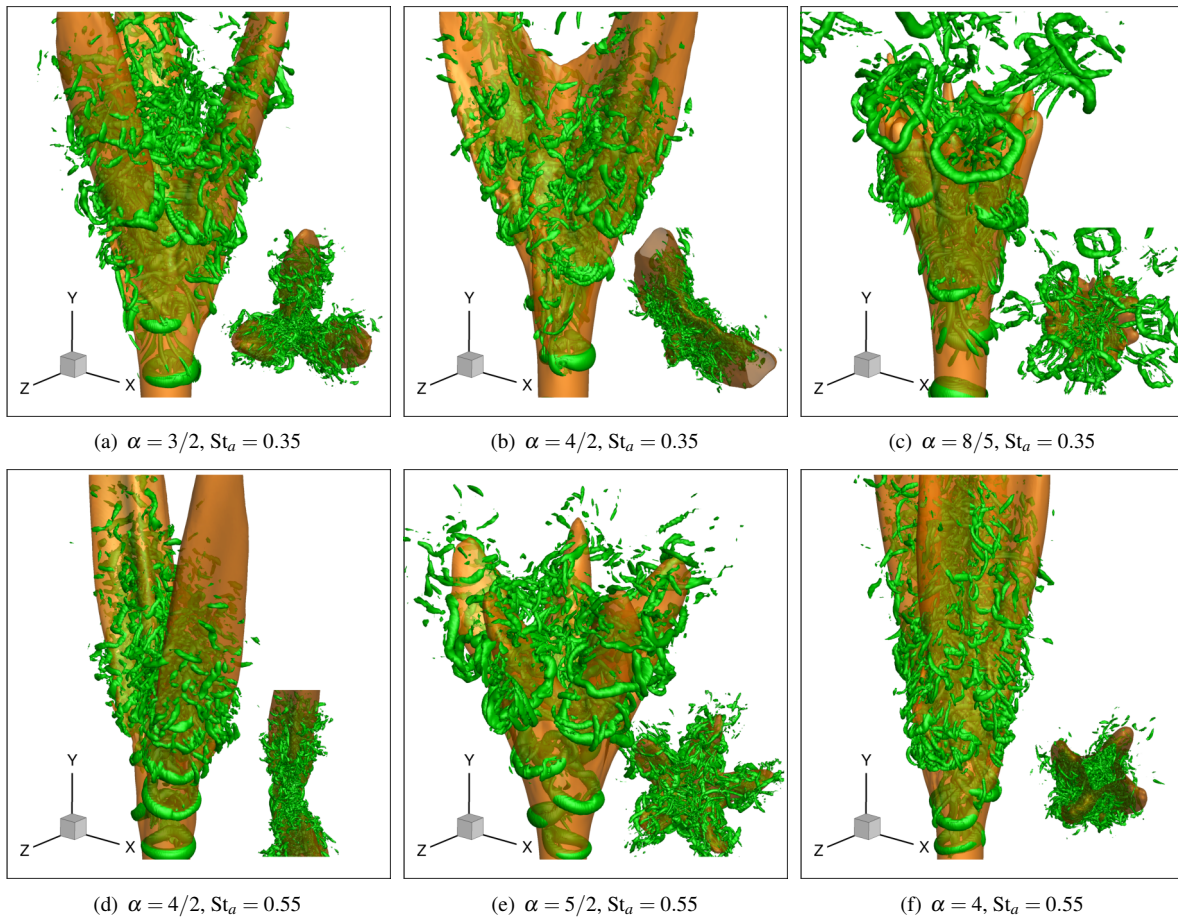
(f) $\alpha = 4$, $St_a = 0.55$

Figure 7. Isosurfaces of the time-averaged axial velocity ($\langle U \rangle = 0.2 U_j$, orange) and instantaneous Q-parameter ($Q = 0.5(U_j/D)^2$, green). The results obtained for $Re = 3000$ with the excitation at $St_a = 0.35$, $St_a = 0.55$ and various α.